A LETTERS JOURNAL EXPLORING THE FRONTIERS OF PHYSICS

OFFPRINT

Electrospinning jets as X-ray sources at atmospheric conditions

P. POKORNÝ, P. MIKEŠ and D. LUKÁŠ

EPL, **92** (2010) 47002

A Letters Journal Exploring the Frontiers of Physics

November 2010

EPL, **92** (2010) 47002
doi: 10.1209/0295-5075/92/47002

www.epljournal.org

Electrospinning jets as X-ray sources at atmospheric conditions

P. Pokorný[(a)], P. Mikeš[(b)] and D. Lukáš[(c)]

Department of Nonwoven Textiles - Nanoscience Centre, Faculty of Textile Engineering, Technical University of Liberec - Studentská 2, Liberec 1, 461 17, Czech Republic, EU

received 29 July 2010; accepted in final form 27 October 2010
published online 2 December 2010

PACS 79.60.-i – Photoemission and photoelectron spectra
PACS 81.07.-b – Nanoscale materials and structures: fabrication and characterization
PACS 52.38.Ph – X-ray, γ-ray, and particle generation.

Abstract – Electrospinning jets producing nanofibres from a polymer solution by electrical forces are fine cylindrical electrodes that create extremely high electric-field strength in their vicinity at atmospheric conditions. However, this quality of electrospinning is only scarcely investigated, and the interactions of the electric fields generated by them with ambient gases are nearly unknown. Here we report on the discovery that electrospinning jets generate X-ray beams up to energies of 20 keV at atmospheric conditions. The X-ray nature of the detected radiation is incontrovertibly proved by a spectroscopic experiment. We hypothesize how the field strength increases to gigantic values in the vicinity of charged electrospinning jets, as a consequence of counterion condensation, to accelerate charged particles, at a short distance, comparable with their mean path at atmospheric pressure, up to kinetic energies that give rise to the detection of X-rays. The experimental set-up designed by us for the generation and detection of high-energy electromagnetic radiation from electrospinning is extremely simple.

The classic way to obtain X-rays is to accelerate thermally emitted electrons from a hot filament in a vacuum discharge tube onto a metallic target [1]. The incident electrons experience either continuous energy losses giving rise to continuous "bremsstrahlung", or to discrete energy losses in the form of "characteristic radiation". Both energy losses of electrons result in X-ray emission. An alternative X-ray source at a moderate vacuum, caused by peeling a roll of common adhesive tape, has been recently described by Putterman *et al.* [2]. Lightning also can generate X-rays with energies of about 10 keV [3–6]. Here, we introduce a method how to generate X-rays of up to 20 keV using an electrospinning set-up without the need for thermally emitted electrons, vacuum environment and metallic target. We hypostatize that the investigated effect of X-rays generation is localized at a microscopic distance from nanofibrous electrodes inside a region of counterion condensation [7–9].

Electrospinning is a recent fibre-forming nanotechnology, which enables us to create submicron fibres drawn from a polymer solution by electrical forces [10–13]. Electrospinners, likewise Röentgen tubes, run at voltages above 30 kV between a spinning electrode, from which the polymer solution is drawn by electric forces, and a collector, on which nanofibres are collected in layers [14], *vide* fig. 1(A). To learn more about the irradiation processes occurring in electrospinning we employed an efficient SLP X-Ray Detector, see fig. 1(B). The detector is protected against discharges generated by the electrospinning jet using a grounded copper grid that serves simultaneously as a screen collector for the produced nanofibres. The morphology of an electrospun nanofibrous layer from aqueous solution of Polyvinyl-alcohol and the fibre diameter distribution are shown in fig. 1(C) and fig. 1(D), respectively.

Typical spectra of X-ray photons emitted from the electrospinning jets as total photon counts accumulated during 150 seconds are shown in fig. 2(A), (B). To exclude noise generated by possible small-scale discharges in the detector the experiment was always run for one minute with switched high-voltage source but without supplying the spinner with a polymeric solution. In this "blind" phase the detector was without any significant signal or noise as documented in fig. 2(C). Spectra "jump up", in successful trials, immediately with the appearance of an electrospinning jet when the needle of the electrospinner is supplied with the polymeric solution. On average, the

(a) E-mail: pavel.pokorny@tul.cz
(b) E-mail: p.mikes@seznam.cz
(c) E-mail: david.lukas@tul.cz

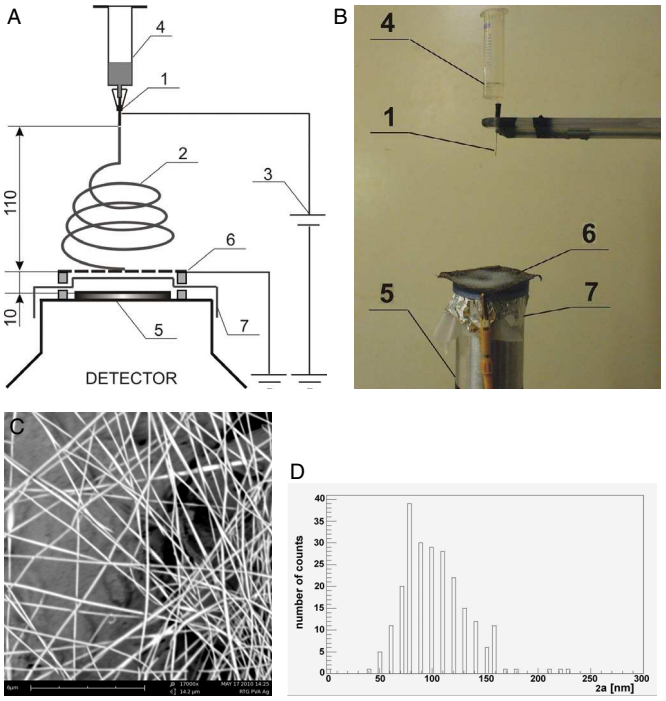

Fig. 1: (Colour on-line) Apparatus for studying high-energy emission from electrospinning. (A, B) Electrospinner consists of a hypodermic needle (1), from which an electrospinning jet (2) is ejected, a high voltage source (3) and a syringe (4) supplying the needle with polymeric solution. The SLP Detector (5) is positioned just behind the grounded screen collector (6). Aluminium foil used in X-rays attenuation experiments (7), *vide* fig. 2(D). The distance between the needle tip and the collector is given in millimetres. (C) The SEM microphotography of the PVA electrospun nanofibrous layer. (D) The fibre diameter, *i.e.* $2a$, distribution.

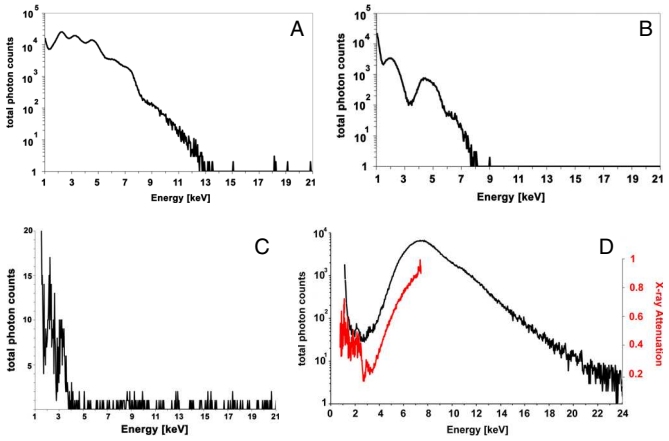

Fig. 2: (Colour on-line) Spectra of X-ray photons emitted from electrospinning jets. (A) Continuous energy spectrum of X-ray total photon counts accumulated during 150 s, vertical scales, emitted from the PVA electrospinning jets recorded by the unshielded SLP X-Ray Detector. The distance between the needle and the collector was adjusted on 110 mm and the voltage was 30 kV. (B) The same spectral measurement done for the 50 mm distance between the needle and the collector and for the voltage 15 kV. (C) A typical detector noise in a "blind" phase of measurement. (D) X-ray attenuation caused by the aluminium foil positioned in-between the screen collector and the detector appears as an absorption slit on the spectrum of total photon counts accumulated during 600 s (the upper curve and the left logarithmic scale). The same distance and voltage as for the (A) case was used. The relative attenuation of the aluminium foil measured using X-ray tube TF 3005/Mo is plotted as the lower curve assigned to the right-hand linear scale.

X-rays signal appears in one out of 15 experimental trials, and then it is quite stable in time. Unsuccessful trials are caused by the creation of thicker or less charged jets and nanofibres that are not able to generate sufficiently severe potential drops for charged particle acceleration.

A thin aluminium foil having a thickness of 0.01 mm and area density of 25 gm^{-2} positioned in-between the screen collector and the detector furnishes the proof about the X-ray nature of the detected events, since the stopping power of the aluminium foil shows itself as an absorption slit on the spectral record of the total photon counts accumulated during 600 seconds in fig. 2(D). The radiation detected in this trial reaches an energy of 20 keV, which is already classified as hard X-rays [15]. A relative attenuation was also measured using the standard X-ray tube TF 3005/Mo, Oxford Instruments, to localize precisely the absorption slit of the employed aluminium shield. The tube is equipped with a molybdenum target having the maximal voltage of 30 kV. It was run at the voltage of 7.5 kV and the maximal current of 0.1 mA during the experiment. The X-ray beam, generated by the tube, was narrowed using an aluminium collimator to the width of 0.5 mm. The relative attenuation, as a ratio of photon counts with and without the aluminium shield, was measured using the Amptek silicon detector XR-100CR, having a sensor area of 6 mm^2 and a width of 0.5 mm. The relative attenuation is plotted as the lower curve in fig. 2(D) assigned to the right-hand linear scale. The figure reveals the identical position of the aluminium attenuation slit at the energy scale in electrospinning and standard X-ray tube experiments.

Electrospinning experiments were carried out using a needle electrospinner equipped with a hypodermic needle of 32 mm length, with an outer diameter of 0.85 mm and an inner diameter of 0.55 mm pointing downwards at the screen electrode called the "collector" on which nanofibres were collected in layers. The screen collector had an area of 50 mm × 50 mm and was made as a grid of copper wires with a diameter of 0.23 mm and with an inner mesh element having 1.07 mm × 1.05 mm area. The collector was grounded while the hypodermic needle was connected to the positive pole of the 300 Watt High Voltage DC Power Supply; model number PS/ER50N06.0-22; manufactured by Glassman High Voltage, INC. with output parameters: 0–50 kV, 6 mA. The fresh 12% wt aqueous PVA solution was prepared by dissolving the polymer in distilled water.

Polyvinyl-alcohol Sloviol-R was purchased from Novacke chemicke zavody, Novaky, Slovakia, having a predominant molecular weight of 60000 g/mol and a dynamic viscosity of 10.4 m Pa s for 4% wt original aqueous solution. An anion surfactant was added into the polymeric solution in 0.5% wt. The beryllium window of the ORTEC SLP-10180P Lithium-Drifted Silicon X-Ray Detector was positioned immediately behind a grounded screen collector of the electrospinner. The detector has its energy range from 30 keV down to 1 keV, and an ultra-thin, 25 μm, beryllium window provides it with an energy resolution, at 5.9 keV photons, of about 180 eV. The temperature during the experiments was 21 °C ± 2 °C and the air relative humidity was 40 ± 5%. The hypodermic needle of the electrospinner was supplied with the polymeric solution at a volume rate of 1 ml/hour using a syringe. This supply rate leads to a production rate of 0.1 ± 0.03 g/hour of the nanofibrous material after the solvent evaporation. The diameter histogram of electrosopun fibres was obtained using FEI® Fibermetric™ System, Powered by PHENOM.

We suggest the following hypothesis to elucidate the observed radiation phenomena: field strength increases to gigantic values in the vicinity of charged electrospinning jets and is able to accelerate charged particles emitted from the jet, *i.e.* electrons and ions, at a short distance comparable with their mean path at atmospheric pressure. Energy losses of these accelerated particles colliding with ambient gas molecules give rise to X-rays. To bring more theoretical evidences we start with a simple model of an asymmetric capacitor in vacuum consisting of a large-plate electrode at a distance h apart from an oppositely charged single cylindrical nanofibre of radius a oriented parallel to the plate, see fig. 3(A). This geometry models an element of an electrospinning jet that serves as an electrode. The electrical potential difference between the plate and the fibre is U. The highest field strength value E_1 on the fibre surface appears on the line of closest points to the plate. The considered physical situation is akin to the analysis of the estimation of the maximal field strength value on the surface of an electric line at a distance h above the ground [16,17] that in the limit $h \gg a$ leads to

$$\frac{E_1}{E_0} = \frac{\xi}{\ln(2\xi)} = Z_1, \qquad (1)$$

where ξ is the dimensionless distance between the fiber and the plate, *i.e.* $\xi = h/a$, while $E_0 = U/h$ denotes the "reference field strength" in a common symmetric two-plate capacitor charged to the potential difference U with the plate-to-plate distance h [18]. The right-hand side of the eq. (1) will be called in the following the "amplifying factor" Z_1, whose dependence on ξ is plotted in fig. 3(B). Adjusting the distance h and the radius a to the values determined from our experiments, *i.e.* $h = 10^{-1}$ m and $a = 5 \times 10^{-8}$ m, the amplifying factor Z_1 reaches a value of 1.3×10^5. The reference field strength value E_0, for the used voltage of 3×10^4 V, is 3×10^5 V/m. Therefore the maximum field strength E_1 is estimated as 39 GV/m,

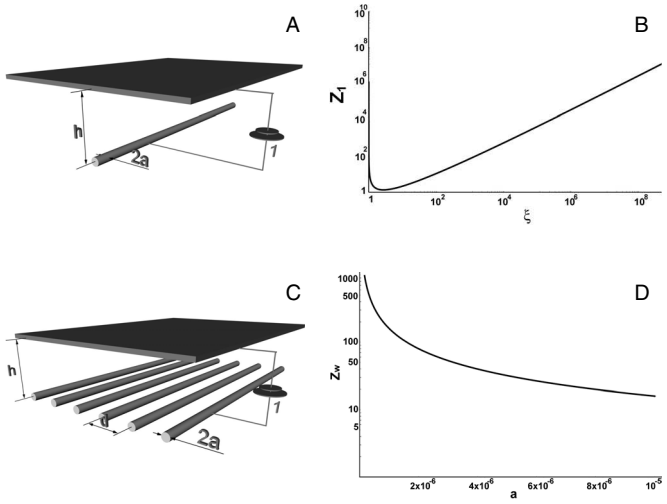

Fig. 3: Asymmetric capacitors and "amplifying factors". (A) The asymmetric capacitor consisting of a large-plate electrode at a distance h from an oppositely charged electrode represented by a single cylindrical fibre with radius a oriented parallel to the plate. A high-voltage source is denoted as (1). (B) The logarithmic plot of the dependence of the "amplifying factor" Z_1 on the dimensionless distance ξ between the fibre and the plate. (C) The asymmetric capacitor composed of a warp of parallel and equidistant nanofibres with a spacing d between neighbouring ones. (D) The relationship between the field strength amplifying factor Z_W and the fibre radius a is calculated for the following parameter values: $h = 10^{-1}$ m, $U = 3\,10^4$ V, $d = 10^{-3}$ m.

which corresponds to the theoretical local surface charge density on the conductive fiber surface reaching the value $\sigma_1 = \varepsilon_0 E_1 = 0.35\,\mathrm{Cm}^{-2}$ and linear charge density $\tau_1 = \pi\varepsilon_0 U/\ln(2\xi) = 5.5 \times 10^{-8}$ C/m, where ε_0 denotes electric permittivity of vacuum. The ions and electrons are accelerated by the field E_1 along a distance x comparable with their mean path in the air at atmospheric pressure, which is about 100 nm [19,20]. The theoretically predicted field strength enables ions and electrons, having elementary charge e, to reach on the distance x a massive kinetic energy, $W_1 \cong E_{\max} \times x \times e$, about 3.9 keV, quite close to the measured X-ray energies in our electrospinning experiments.

In contrast to one isolated fibre perfectly parallel with the counterpart electrode, our experiments were carried out with gyrating and coiling the electrospinning jet that is modelled further as a warp-like pattern of fibres, *vide* fig. 3(C). The existence of neighbouring fibres in the fibrous warp tends to decrease the maximum field strength. The amplification factor Z_W for a warp of parallel and equidistant nanofibres with a spacing d between neighbouring ones, as sketched in fig. 3(D), is governed by the dimensionless distance $\rho = d/a$, if $h \gg d \gg a$, and is nearly independent of h [18]:

$$\frac{E_W}{E_0} \cong \frac{\rho}{2\pi} = Z_W, \qquad (2)$$

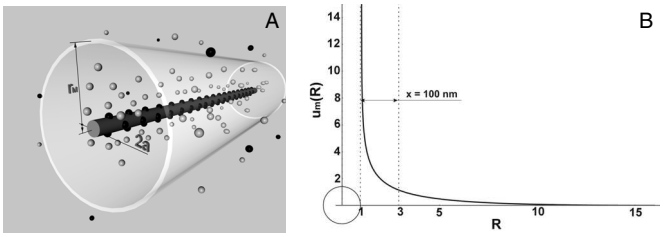

Fig. 4: The Manning region and dimensionless potential inside it. (A) Counterions, light-gray particles, prevail absolutely inside the Manning region, sketched as a transparent outer cylinder, in the vicinity of a charged fibre. Rest counterions and oppositely charged ions, dark-gray particles, dilute away to infinity forming the Debye-Hückel region. (B) Relationship between the dimensionless potential u_M and the dimensionless distance R inside the Manning region. The cross-section of a fibre with dimensionless radius 1, being 50 nm in reality, and the adjacent area of the anomalous field strength values up to $x = 100\,\mathrm{nm}$ are schematically inserted into the graph.

where E_W is the maximal field strength value on the surface of one of the warp fibers. Estimating the maximal inter-fiber distance d in a real electrospinning jet as 0.1 mm, one obtains $\rho = 2 \times 10^3$ and the amplifying factor as $Z_W \cong 3.2 \times 10^2$. The maximum field strength E_W is estimated as 0.095 GV/m and the linear charge density as $\tau_W \cong \pi\varepsilon_0 U/(2\pi\zeta) = 1.3 \times 10^{-9}\,\mathrm{C/m}$ for conductive fibers, where $\zeta = h/d$. The predicted field strength enables electrons and univalent ions to reach at atmospheric conditions a kinetic energy W_W of about 0.0095 keV, which is roughly three orders less than the maximal X-ray energy in measured spectra.

However, a massive amplification of the field strength in the vicinity of an electrospinning jet or a nanofibre is due to the effect of "counterion condensation", which is a well-known effect in polyelectrolytes [9]. The condensation appears, as discussed in [18], when the dimensionless linear charge density q on a tiny nanofiber-like cylindrical body exceeds its critical value, *i.e.*, $q \gg 1$. Counterion condensation erases the decay of field strength caused by grouping nanofibres into warps. Counterions "condense" in the immediate vicinity of the cylindrical fiber forming the so-called Manning region having a diameter r_M [21,22], *vide* fig. 4(A). According to Kornev [23], the Manning region spans up to the maximal dimensionless radius $R_M = r_M/a \cong 16407$ for $q \to \infty$. A dense cloud of couterions plays the role of a counterelectrode positioned in the immediate proximity of the oppositely charged jet. Therefore, the field strength reaches gigantic values between them. A dimensionless potential $u_M(R)$ inside the Manning region has a severe "double-logarithmic" decay [18]:

$$u_M(R) = -\ln\left[\left(\frac{\kappa a}{2z}\right)^2 R^2 \cos^2\left(z \ln\frac{R}{R_M}\right)\right], \qquad (3)$$

where κ^2 is the dimensionless Debye-Hückel parameter, R denotes the dimensionless radial distance from the jet axes, *i.e.*, $R = r/a$, and z is defined as $z \cong \exp(-C_E)$ [23]. The constant $C_E = 0.577215\ldots$ is Euler's constant.

The dimensionless potential value $u_M(1)$ on the surface of a jet is supposed to be $(3 \times 10^5\,\mathrm{V}) \times e/(k_B T)$ in our experiments and plays the role of a boundary condition. The drop of the dimensionless potential $u_M(R)$ with an increasing distance from the fiber surface is enormously rapid and the potential reaches a negligible value at a distance shorter than the particle mean path at atmospheric pressure, *vide* fig. 4(B).

The theoretically predicted potential drop enables electrons or ions to reach over the short distance $x \cong 100\,\mathrm{nm}$ a massive kinetic energy

$$W_M \cong [\varphi(a) - \varphi(a+x)] \times e, \qquad (4)$$

which is about 15 keV. This estimation is in broad agreement with the measured maximal X-ray energy in the spectra obtained from electrospinning experiments. The difference between the estimated and measured maximal energies is explained as a consequence of ion density fluctuations inside the Manning region. The roughly estimated mean-field strength value E_M is about 150 GV/m, since the potential $\varphi(r)$ loses one-half of the voltage applied, *i.e.*, 15 kV, along the distance $x \cong 100\,\mathrm{nm}$. The field strength is anomalous only in the closest vicinity of a nanofibre, therefore avalanches of the created ions caused by subsequent ionic collisions do not take place here, and therefore a typical corona is not ignited. Such field strength value is sufficient for gas phase ionization of deuterium (>25 GV/m) and undoubtedly it causes ionization of neutral air molecules nearby a jet [24].

Ions or electrons, kicked by an increasing chemical potential inside the thinning electrospinning jet into the region of condensed counterions, can be significantly accelerated by the predicted gigantic field strength at a distance x of their mean path in the air at atmospheric pressure. The total energy radiated by one accelerating electron at these conditions is, according to Larmor formula, less than 0.0001% of the obtained kinetic energy and hence relativistic effects are negligible.

The closest vicinity of individual nanofibrous jets in our experimental setup operates, according to our hypothesis, as a "nanoscopic" particle accelerator acting over unusually short distances at gigantic field strength values restricted to the vicinity of a nanofibrous electrode. Thanks to the space restriction of the anomalous field strength values to distances of about 100 nm, the typical corona is not ignited. Accelerated particles ejected outside the jets due to the Kelvin-Thompson law collide with other gas particles inside the Manning region, including ions, or with other materials within their reach, giving rise to electron- or particle-induced X-rays. The investigated effect could find its applications in a lot of fields. For instance: portable X-ray sources for therapeutic and analytical purposes and the design of anomalous particle accelerators in nuclear physics including fusion apparatuses [24]. This investigation could

provide also an important new insight into the mechanism for generating X-rays from lightning and long laboratory sparks.

* * *

The main support for this research was provided by The Ministry of Interior of the Czech Republic, program BV II/2-VS, grant No. 1656, "Nanomaterials to persons protection against CBRN substances". DL is also thankful to the Fulbright Scholar Program 2009/2010. PM has been supported by GACR, grant No. 102/08/H081 "Unusual application of physical fields". PP is thankful for the support from the "Research Centre Texlile II" (the project MPO CR FT-TA3/017). The authors feel obliged to K. Kornev from the School of Materials Science and Engineering, Clemson University, SC and A. Kopal from Department of Physics, Technical University of Liberec for a lot of useful discussions. We are very grateful to T. Čechák and T. Trojek from the Czech Technical University in Prague, Faculty of Nuclear Sciences and Physical Engineering, specifically, for their invaluable assistance with the spectral measurements. The authors also thank Cummins Filtration for their interest in this work. The authors declare that they have no competing financial interest and that they contributed equally to this work.

REFERENCES

[1] Stanton A., *Nature*, **53** (1896) 274.
[2] Mamara C. G., Escobar J. V., Hird J. R. and Putterman S. J., *Nature*, **455** (2008) 1089.
[3] Black R. A. and Hallett J., *Am. Sci.*, **86** (1998) 526.
[4] Dwyer J. R. *et al.*, *Science*, **299** (2003) 694.
[5] Gurevich A. V. and Zybin K. P., *Usp. Fiz. Nauk*, **44** (2001) 1119.
[6] Gurevich A. V., Milib G. M. and Valdivia J. A., *Phys. Lett. A*, **23** (1997) 402.
[7] Manning G. S., *J. Chem. Phys.*, **51** (1969) 924.
[8] Manning G. S., *J. Chem. Phys.*, **51** (1969) 934.
[9] Manning G. S., *J. Chem. Phys.*, **51** (1969) 3249.
[10] Reneker D. H. and Yarin A. L., *Polymer*, **49** (2008) 2387.
[11] Filatov Y., Budyka A. and Kirichenko V., *Electrospinning of Micro- and Nanofibers: Fundamentals in Separation and Filtration Processes* (Begell House, Redding) 2007.
[12] Andrady A. L., *Science and Technology of Polymer Nanofibres* (Wiley, Hoboken, NJ) 2008.
[13] Hohman M. M., Shin M., Rutledge G. and Brenner M. P., *Phys. Fluids*, **13** (2001) 2201.
[14] Lukas D. *et al.*, *Text. Prog.*, **41** (2009) 59.
[15] Lovesey S. W. and Collins S. P., *X-ray Scattering and Absorption by Magnetic Materials* (Oxford University Press) 1996.
[16] Landau L. D. and Lifshitz E. M., *Electrodynamics of Continuous Media* (Elsevier, Amsterdam) 2008.
[17] Jeans J. H., *The Mathematical Theory of Electricity and Magnetism* (Cambridge University Press, Cambridge) 1911.
[18] Supplementary information: `www.knt.tul.cz`→download→ europhysics, figs. SI 1 and SI 2, references.
[19] Avallone E. A., Baumeister T., Sadegh A. and Marks L. S., *Marks' Standard Handbook for Mechanical Engineers* (McGraw-Hill Professional) 2006.
[20] Grigor'ev A. I. and Skinevich O. A., *Sov. Phys. Tech. Phys.*, **29** (1984) 735.
[21] Zimm B. H. and Le Bret M. J., *J. Biomol. Struct. Dyn.*, **1** (1983) 461.
[22] Tracy C. A. and Widom H., *Physica A*, **244** (1997) 402.
[23] Kornev K., *Phys. Rev. E*, **60** (1999) 8554.
[24] Naranjo B., Gimzewski J. K. and Putterman S., *Nature*, **434** (2005) 1115.